J. Anal. Appl. Pyrolysis 85 (2009) 260–267

Contents lists available at ScienceDirect

Journal of Analytical and Applied Pyrolysis

journal homepage: www.elsevier.com/locate/jaap

Biomass pyrolysis: Kinetic modelling and experimental validation under high temperature and flash heating rate conditions

Capucine Dupont [a,*], Li Chen [a], Julien Cances [a], Jean-Michel Commandre [b], Alberto Cuoci [c], Sauro Pierucci [c], Eliseo Ranzi [c]

[a] CEA, 17 rue des Martyrs, 38054 Grenoble cedex 09, France
[b] RAPSODEE, UMR-CNRS 2392, Ecole des Mines d'Albi-Carmaux, 81013 Albi CT cedex 9, France
[c] CMIC Politecnico di Milano, Piazza Leonardo da Vinci, 32, 20133 Milano, Italy

ARTICLE INFO

Article history:
Received 30 June 2008
Received in revised form 18 November 2008
Accepted 19 November 2008
Available online 3 December 2008

Keywords:
Biomass
Pyrolysis
Modelling
Devolatilization
Gas phase kinetics
Entrained flow reactor

ABSTRACT

This work analyzes and discusses the general features of biomass pyrolysis, both on the basis of a new set of experiments and by using a detailed kinetic model of biomass devolatilization that includes also successive gas phase reactions of the released species and is therefore able to predict the main gases composition. Experiments are performed in a lab-scale Entrained Flow Reactor (EFR) to investigate biomass pyrolysis under high temperatures (1073–1273 K) and high heating fluxes (10–100 kW m^{-2}). The influence of particle dimensions and temperature has been tested versus solid residence time in the reactor. The particle size appeared as the most crucial parameter. The pyrolysis of 0.4 mm particles is nearly finished under this range of temperatures after a reactor length of 0.3 m, with more than 75 wt% of gas release, whereas the conversion is still under evolution until the end of the reactor for larger particles up to 1.1 mm, due to internal heat transfer limitations. The preliminary comparisons between the model and the experimental data are encouraging and show the ability of this model to contribute to a better design and understanding of biomass pyrolysis process under severe conditions of temperature and heating fluxes typically found in industrial gasifiers.

1. Introduction

Biomass is a renewable, CO_2-neutral energy resource, widely available and increasingly used as an alternative to fossil fuel for energy supply. The thermal conversion of biomass to produce fuel gas (mainly CO and H_2) via gasification, of which pyrolysis is the first step, is considered as a very promising process. It is well known that biomass pyrolysis is a complex process that involves mass and heat transfer phenomena as well as chemical reactions. Furthermore, the chemical reactions during pyrolysis can be focused on three different aspects:

- Biomass devolatilization: i.e. the decomposition of the solid into permanent gases, condensable vapours (*tars*) and solid residue (*char*);
- Secondary gas phase reactions of the released gas and tar species;
- Heterogeneous reactions between solid and gas.

The way these reactions occur, and therefore the final product yield, is strongly related to operating conditions and possible heat and mass transfer resistances. Several researchers have studied the intrinsic kinetic of biomass devolatilization with small particles (~100 μm). Network biomass devolatilization models describe accurately the chemistry of the devolatilization process [1]. The FG (functional group)-Biomass model [1–3], the Bio-Flashchain model [4], and the bio-CPD (chemical percolation devolatilization) model [5,6] are examples of these network models. They assume that the biomass macromolecule is constituted of different lumped groups, and the macromolecular fuel structure changes during the devolatilization process to produce gas, tar, and char. These models, initially developed for coal devolatilization, have been recently extended to biomasses, but their availability and validation are still limited. Research efforts have also been devoted to the pyrolysis of large (said as "thermally thick") biomass particles [7–10] in order to study the influence of heat and mass transfer limitations and the evolution of solid physical properties. Usually the chemistry of biomass devolatilization is roughly sacrificed. As clearly stated by Di Blasi [11], as well as by Janse et al. in modelling the flash pyrolysis of a single wood particle [12], the accurate knowledge of the reaction kinetics appears to be a crucial parameter for a reliable modelling of the pyrolysis process.

Besides, the main conclusion of a recent literature review on the modelling of biomass pyrolysis [13,14] underlines that the available knowledge on kinetics and transport phenomena has

* Corresponding author.
E-mail address: capucine.dupont@cea.fr (C. Dupont).

0165-2370/$ – see front matter © 2008 Elsevier B.V. All rights reserved.
doi:10.1016/j.jaap.2008.11.034

Nomenclature

A	reactor cross-section [m^2]
C	species concentration [mol m^{-3} s^{-1}]
C_P	specific heat [J kg^{-1} K^{-1}]
d_P	particle diameter [m]
f	friction factor
g	gravity [m s^{-2}]
h	species enthalpy [J kg^{-1}]
J	particle mass flux [kg s^{-1}]
K	global mass exchange coefficient [m s^{-1}]
m	mass of particle sector [kg]
$\dot{m}$	total mass flow rate of particles [kg s^{-1}]
m_P	particle mass [kg]
M	species molecular weight [kg $kmol^{-1}$]
NC	number of species
NR	number of reactions
NS	number of particle sectors
q	heat flux from particle to gas phase [J s^{-1}]
r	reaction rate [kmol m^{-3} s^{-1}]
S	external surface of particle sector [m^2]
t	time [s]
U	global thermal exchange coefficient [W m^{-2} K^{-1}]
v	velocity [m s^{-1}]
V	volume of spherical sector [m^3]
W	gas phase mass flow rate [kg s^{-1}]
z	reactor axial coordinate [m]

Greek letters

α	thermal diffusivity [m^2 s^{-1}]
Γ	mass diffusivity [m^2 s^{-1}]
ΔH	reaction heat [J mol^{-1} s^{-1}]
ε	porosity
η	total concentration of solid particles [#/m^{-3}]
λ	thermal conductivity [J m^{-1} s^{-1} K^{-1}]
ξ	radial coordinate [m]
ρ	density [kg m^{-3}]
υ	stoichiometric coefficient

not been integrated properly for reactor design. Accurate measurements are difficult, mass balance closures are seldom good enough to determine the trends of the product yields as a function of temperature and biomass particle size. Unfortunately, it appears that the reaction kinetics reported until now cannot be used to predict the product distribution with enough accuracy. These conclusions emphasize the value of new experimental measurements and new research activity on these topics.

In the present study, a lab-scale Entrained Flow Reactor (EFR) has been used to study experimentally the pyrolysis behaviour of biomass particles under severe conditions, namely high temperatures (1050–1250 K) and high heating fluxes (10–100 kW m^{-2}). Then the experimental results are used to further compare with the prediction of a semi global kinetic model of biomass pyrolysis in order to test its predicting ability under EFR conditions. The model [15] includes a description of the chemistry of biomass devolatilization and a detailed scheme of successive gas phase reactions, which is able to predict not only the total yields of gas, tar, and char, but also the yields of individual species released in gas phase.

2. Experimental work

2.1. Experimental facility

The lab-scale entrained flow reactor used in this study is depicted in Fig. 1. The reactor consists in an alumina tube of 0.075 m internal diameter heated by an electric oven that can reach a maximum temperature of 1300 K. Pure N_2 is injected at the top of the reactor and then passes through an electric pre-heater. A constant flow rate of solid is injected at the top of the reactor by pneumatic transport (flow rate of N_2 equal to 2 L min^{-1} (STP)) in a cooled tube. At the end of the tube, the cold solid particles are distributed homogeneously over the reactor cross-section thanks to a dispersion dome and suddenly enter in contact with the hot gas. The gas flow rate is 16 L min^{-1} (STP), and the solid flow rate is 0.5 and 1 g min^{-1} for beech wood and mixture of Scot pine and spruce, respectively. Under the explored conditions, the gas flow is highly laminar ($Re < 200$). The reactor is isothermal in the zone between 0.30 and 0.95 m away from the solid injection.

A cooled sampling probe is placed from the bottom at different altitudes inside the reactor for gas and solid analyses. Thus the gas and solid residence times can be varied inside the reactive zone. The samples are sent to a decanter where the solid is collected. Then the gas mixture is sent to a filter that retains fine particles and most remaining tars. At last, the gas is analyzed by several analyzers:

- A microgas chromatography (H_2, CO, CO_2, CH_4, C_2H_4, C_2H_2, C_2H_6);
- A Fourier Transform Infra Red spectrometer (CO, CO_2, CH_4, C_2H_4, C_2H_2, C_2H_6);
- A Non-Dispersive Infrared analyzer (O_2 , CO_2);
- Two Flame Ionization Detectors (CH_4, total hydrocarbons);
- A Thermal Conductivity Detector (H_2);
- A hygrometric mirror (H_2O contained in gas at ambient temperature).

Note that each gas component is measured at least by two analyzers. The differences between the measurements are always below 5% of the value.

The mass balance was checked for several experiments by measuring both gases and solids at the outlet of the reactor, as explained in [16]. Most of the products can be found in the measured wet gas, with values higher than 75–80 w%. About 10–15 w% can be found in the solid and about 5–10 w% of the initial mass is lacking for a complete closure of the balance. It is expected that a significant part of this 10 w% may be attributed to unmeasured tars. This is coherent with our experimental observations and similar experiments found in the literature [17,18].

2.2. Biomass samples

Two woody biomasses were used for the experiments: a mixture of softwoods (Scot pine and spruce) and beech. For the mixture of pine and spruce, two particles sizes were used:

(i) 355–530 μm (average diameter of 0.4 mm);
(ii) 1.00–1.25 mm (average diameter of 1.1 mm).

For the beech wood, four ranges of particle sizes were used:

(i) 100–313 μm (average diameter of 0.2 mm);
(ii) 400–500 μm (average diameter of 0.45 mm);
(iii) 630–710 μm (average diameter of 0.67 mm);
(iv) 800–900 μm (average diameter of 0.85 mm).

The data on biomass samples, measured following the usual standards, are given in Table 1.

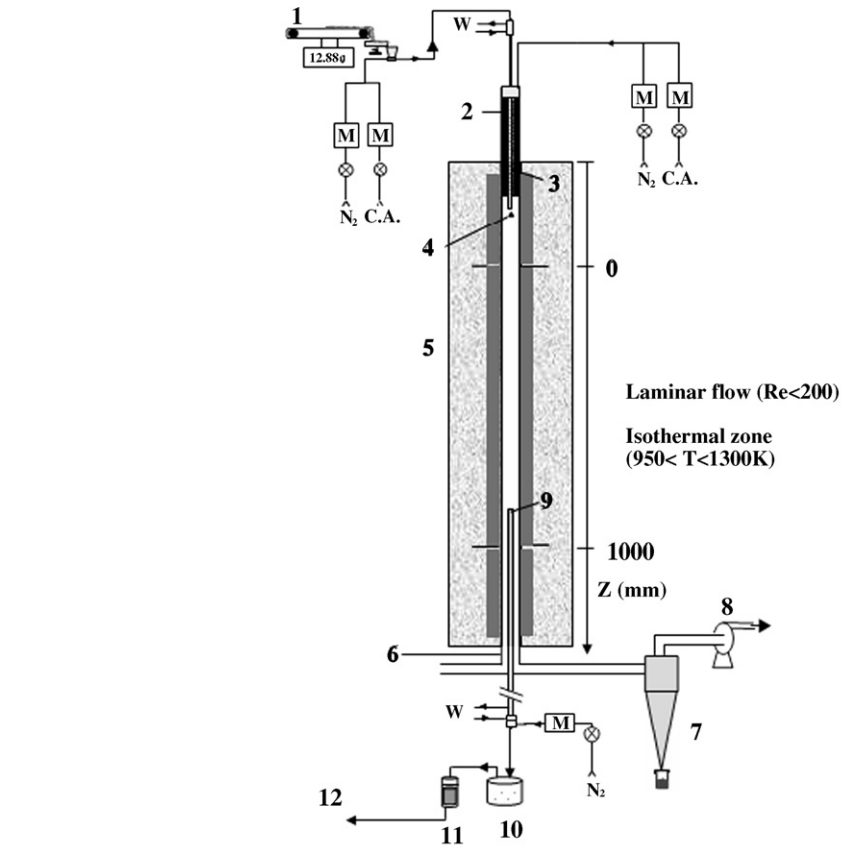

Fig. 1. Scheme of the Entrained Flow Reactor (EFR).

3. Mathematical model

The main objective of this modelling analysis is to better understand the overall performance of the Entrained Flow Reactor (EFR) where biomass pyrolysis is carried out. The specificity of the numerical model used here is to focus the attention not only on the description of mass and heat transfer processes at the particle and reactor scales, but also on the chemistry of biomass devolatilization.

Three main sub-models, which will be briefly described in this section, are combined to obtain the global mathematical model of the EFR:

Table 1
Ultimate and proximate analysis of biomass samples.

			Scot pin and spruce		Beech wood			
		Units	0.4 mm	1.1 mm	0.2 mm	0.45 mm	0.67 mm	0.85 mm
Ultimate analysis	Carbon	wdaf%[a]	48.6	50.5	49.2	49.2	49.2	49.2
	Hydrogen	wdaf%	6.0	6.25	6.0	6.0	6.0	6.0
	Nitrogen	wdaf%	0.2	0.1	0.5	0.5	0.5	0.5
	Sulfur	wdaf%	0.03	0.02	0.02	0.02	0.02	0.02
	Oxygen	wdaf%	43.0	43.1	44.3	44.3	44.3	44.3
Proximate analysis	Moisture	w%	7.2	8.6	6.5	6.4	7.2	7.5
	Volatile matter	wdf%[a]	77.0	77.4	85.6	85.6	85.3	85.2
	Fixed carbon	wdf%	20.9	21.9	14.0	14.0	14.4	14.4
	Ash	wdf%	2.1	0.6	0.4	0.4	0.3	0.3
	Particle density	kg m^{-3}	300	450				

[a]wdf%: mass dry free. wdaf%: mass dry ash free.

1. The kinetic model of biomass pyrolysis;
2. The biomass particle model;
3. The reactor model.

3.1. The kinetic model of biomass pyrolysis

As already discussed in a previous paper [19], thermodynamic and equilibrium models are not accurate enough to design biomass gasifiers. They overestimate the yield of H_2 and CO, underestimate the yield of CO_2 and predict a gas nearly free of CH_4 and heavier species. Empirical correlations are needed to improve these predictions with the corresponding limitations of reliability and applicability [20,21]. As a consequence, mechanistic models of biomass pyrolysis and gasification need to be applied at the particle scale with inclusion of the successive reactions of released species in order to account for the gas-phase kinetics. Beside heat and mass transport processes, a mechanistic model of biomass gasification and pyrolysis should focus on three different facets of the overall process:

1. Biomass devolatilization, i.e. the decomposition of the solid into permanent gases, condensable vapors (*tars*) and solid residue (*char*);
2. Successive or secondary gas phase reactions of the released gas and tar species;
3. Heterogeneous reactions between solid and gas, that are usually much slower than the previous stages [19]

The kinetic mechanism very recently proposed by Ranzi et al. [15] is here applied: it describes both the chemistry of biomass devolatilization and successive gas phase reactions. Biomasses are simply characterized in terms of cellulose, hemicellulose and lignin, whose respective amounts, if not available on the basis of an experimental biochemical analysis, can be directly derived on the basis of the elemental composition (C, H and O). A multi-step kinetic model defines the rates and the stoichiometry of a few lumped reactions, for each reference component. The overall devolatilization of biomass particles is then the combination of the decomposition of reference components. After this first step, all the released species in the gas phase are then described with their primary propagation and decomposition reactions in the gas phase. This sub-set of elementary and lumped gas phase reactions is coupled with a more general and detailed kinetic scheme of pyrolysis of hydrocarbon species, from methane up to kerosene and diesel fuels [22]. The model is therefore able to account for the successive evolution of the species in the gas-phase and to predict the final products, mainly H_2, CO, CO_2, CH_4, C_2 and H_2O. The whole reaction scheme, constituted by 132 molecular and radical species involved in 2808 elementary and lumped reactions, is available online in CHEMKIN format at www.chem.polimi.it/CRECKModeling/.

As far as the kinetics of gasification of char residue is concerned, it is assumed that the solid residue is pure carbon and usual kinetic laws are then used [23]. Possible different char composition and/or catalytic effect of metal contained in the ash residue could be tackled with empirical correction factors. Note that these reactions are much too slow to occur under the conditions of the present experiments, as shown by Dupont et al. [16].

3.2. The biomass particle model

The biomass particle model is based on mass and energy balances over the particle and gas phase boundary conditions. The complexity of these models strongly depends on the description level of the time evolution of the solid matrix. On the basis of this transformation, the physical properties of the solid and the transport properties of the diffusing gases are derived [7].

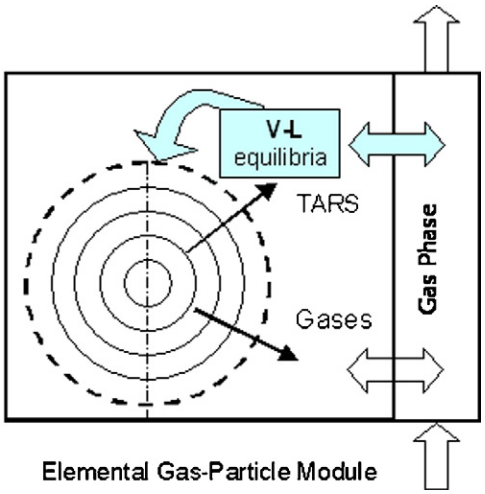

Fig. 2. Scheme of the elemental gas-particle module.

A simplified scheme of the elemental gas-particle module indicating the gas–solid interactions and the release of *tar* components is reported in Fig. 2.

The biomass particle, which consists of a mixture of reference components and ash, is assumed as a homogeneous sphere with NS internal sectors that account for possible heat and mass transfer resistances. Gases are released by the particle to the surrounding gas phase while surrounding gases diffuse into the solid particle.

The mass balance for the *i*th species in the *j*th spherical sector is given by

$$\frac{dm_{j,i}}{dt} = J_{j-1,i} - J_{j,i} + (1-\varepsilon_j)V_j M_i \sum_{k=1}^{NR_{part}} (\upsilon_{i,k}^{part} \cdot r_{j,k}^{part}) \quad (1)$$

The contribution to mass flow rate $J_{j,i}$ in the mass balance equation results

$$J_{j,i} = -\Gamma_{j,i} \left.\frac{dC_{j,i}^{part}}{d\xi}\right|_{r_j} \cdot S_j \cdot \varepsilon_j \quad (2)$$

The flux exchanged with the gas phase at the external surface is

$$J_i^{DEV} = K_i (C_{NS,i}^{part} - C_i^{gas}) \cdot S_{NS} \cdot \varepsilon_{NS} \quad (3)$$

The energy balance for the *j*th spherical sector includes the conduction term, the enthalpy contributions associated to the mass fluxes and the reactions duties

$$\frac{d}{dt}(m_j C_{P_j}^{part} T_j^{part}) = -\lambda_{j-1}^{part} \left.\frac{dT_j^{part}}{d\xi}\right|_{r_{j-1}} S_{j-1} + \sum_{i=1}^{NC} J_{j-1,i} h_{j-1,i}^{part} + \lambda_j^{part} \left.\frac{dT_j^{part}}{d\xi}\right|_{r_j} S_j - \sum_{i=1}^{NC} J_{j,i} h_{j,i}^{part} + \sum_{k=1}^{NR_{gas}} (-\Delta H_{j,k}^{part} \cdot r_{j,k}^{part}) \quad (4)$$

where the last term is the total heat production rate due to chemical reactions.

The heat exchanged with the gas phase at the external surface ($j = NS$) is

$$q = U(T_{NS}^{part} - T^{gas}) \cdot S_{NS} \quad (5)$$

Released *tar* components can either mix with the surrounding gases or, at lower temperatures, can condensate on cold surfaces.

Gas phase is considered as a perfectly stirred reactor inside the cell module. Convective fluxes or flow rates entering and exiting the module are allowed, both for gas and solid phase. This elemental module is flexible and suitable for simulating different process alternatives, such as fixed or moving bed gasifiers and combustors, updraft or downdraft configurations and also the entrained flow reactor. The C++ BzzDAE solver is used to numerically handle this mathematical model [24,25]. Physical and mathematical details on the overall complexity of this problem are given elsewhere [26].

3.3. Mathematical model of the lab-scale entrained flow reactor

Here is briefly described the way how the particle model is applied to the Entrained Flow Reactor. The emphasis is mainly put on the characterization along the reactor of two crucial parameters:

- The particle velocity
- The heat and mass transfer coefficients between the particle and the surrounding gases.

Gas and solid particles move with different velocity inside the EFR. The slip velocity $|v^{gas} - v^{part}|$, i.e. the relative velocity of gas and solid particle, needs to be properly calculated in order to account not only for the contact times inside the reactor, but also for the proper assessment of heat and mass transfer coefficients. The gas velocity v^{gas} is practically constant along the whole reactor and is about 0.28 m/s in the current experiments. The particle velocity v^{part} is derived from the momentum balance equation on the single particle, accounting for buoyancy and drag forces.

The slip velocity for the 0.2 mm particles asymptotically approaches the value of ~0.20 m/s after ~0.15 m from the injection zone and the corresponding particle residence time t_P inside the reactor is about 2 s. The slip velocity for the 1.1 mm particles at the reactor outlet is more than 2 m/s with a corresponding residence time of less than 0.5 s. Further details on these calculations are reported elsewhere [27].

The mass balance equation of the ith gas phase species inside the EFR is given by

$$\frac{dW_i^{gas}}{dt_P} = v^{part} \cdot A \left[\eta \cdot J_i^{DEV} + M_i \sum_{k=1}^{NR_{gas}} (\upsilon_{i,k}^{gas} \cdot r_k^{gas}) \right] \quad (6)$$

where the total concentration of solid particles in the gas phase can be expressed as

$$\eta = \frac{\dot{m}}{v^{part} \cdot A \cdot m_P} \quad (7)$$

Energy balance equations of the solid and gas phases are treated with the same assumptions already described for the mass balance equations. The gas enthalpy balance becomes:

$$\frac{d}{dt_P}(W_G \cdot C_P^{gas} \cdot T^{gas}) = v^{part} \cdot A \left[\left(\sum_{k=1}^{NR_{gas}} (-\Delta H_k^{gas} \cdot r_k^{gas}) \right) + \eta \left(\sum_{i=1}^{NC} J_{i,NS}^{DEV} h_{i,NS}^{part} + q \right) \right] \quad (8)$$

Due to the continuous variation of the slip velocity, the effective heat transfer coefficient is also varying along the entire reactor. These values are calculated by taking into account the effect of convection [28], radiation and the proper correction due to the significant mass fluxes directed towards the gas phase [29] and the relative cold product vapors reducing the penetration of heat into the particle. This calculation leads to average values of about 650 and 250 $W\,m^{-2}\,K^{-1}$ for the smallest and largest particles, respectively.

4. Comparison between experimental data and model predictions

4.1. General trends

Model predictions allow to describe the devolatilization process in its different facets. Fig. 3 shows the predicted evolution of the decomposition of cellulose, hemicellulose and lignin species for mixture of pine and spruce (0.4 mm) at 1073 K. Note that two different lignins have been used to better distinguish hardwood and softwood lignins [15]. The decomposition begins after about 0.15 m from the injection dome and temperatures higher than 800 K. It moves through different intermediates up to the final formation of the *char* residue. The decomposition seems to be nearly finished after 0.5 m under these conditions.

In agreement with the experimental results on char shown in Fig. 3, the char yield reaches values of 14–16 wt% of the initial dry biomass. According to the model, the initial composition of the biomass $C_6H_{8.8}O_{3.9}$ significantly changes at the reactor outlet and becomes $C_6H_{2.9}O_{1.1}$ at 1073 K; at 1223 K, the charification process is further completed and the composition of the solid residue becomes $C_6H_{1.4}O_{0.5}$. These results are in accordance with the experimental measurements indicating a composition of $C_6H_{2.7}O_{0.8}$ at 1073 K and $C_6H_{1.5}O_{0.4}$ at 1223 K.

The release of the major *tar* components and their successive decomposition to form the final gas products can also be predicted by the model with a large detail, as shown in Fig. 4. The presence of tar species could not be measured but was also experimentally observed, in terms of depositions and fouling on the surface of the sampling probe. During experiments made at low temperature (1073 K) and contact times corresponding to a reactor length of 0.2–0.3 m, the sampling probe was fouled by sticky material. This observation is in agreement with the maximum in the *tar* fractions predicted by the model, as shown in Fig. 4.

Since the elemental composition of the two woods is the same, the same kinetic parameters (which are derived from the elemental compositions of the initial biomass) have been used in the model. This is in agreement with the experimental measurements reported in Table 2 for 0.4 mm particles of the two different biomasses treated under the same operating conditions (T = 1073–1223 K; reactor length: 0.9 m) for which

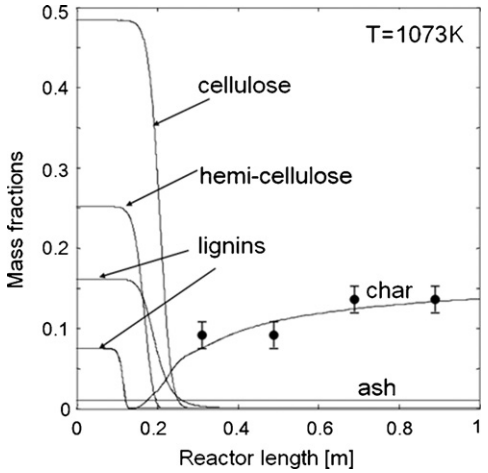

Fig. 3. Modelling results for the decomposition of the biomass reference species and comparison between experimental measurements and modelling results for char yield (softwood particles of 0.4 mm at 1073 K).

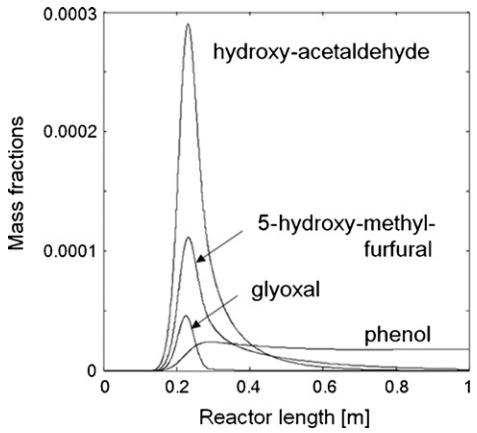

Fig. 4. Modelling results on the relevant tar components in the gas phase (softwood particles of 0.4 mm at 1073 K).

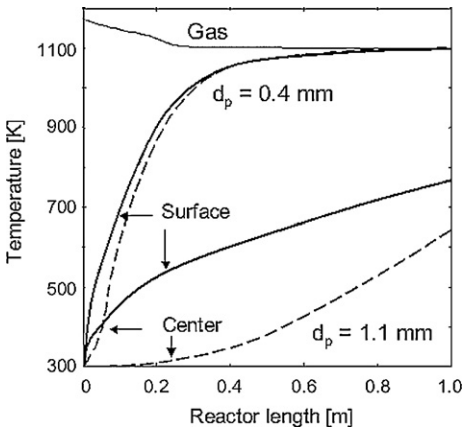

Fig. 5. Surface and inner solid temperatures along the reactor length (softwood particles of 0.4 mm at 1073 K).

the decomposition is finished. Indeed it can be seen that the products yields are nearly the same for the two samples.

The agreement between model and experiments is good on practically all the species, except H_2. The wet gas yield is higher than 75 w% for 0.4 mm particles under these conditions of temperature (1073 K–1273 K). CO is largely the main product of the gas, followed by H_2 and H_2O. CH_4 and CO_2 are present in lower amounts. Hydrogen over prediction (mainly at low temperature) seems mainly due to the secondary pyrolysis reactions in the gas phase: tar components rapidly decompose in the gas phase forming significant amounts of intermediate species (C_2H_6, C_2H_5OH, CH_2O...) subject to successive dehydrogenation reactions. This over prediction needs to be better analyzed, both at the level of the primary chemistry of biomass devolatilization and for the secondary gas phase pyrolysis. Some experimental bias may also be suggested to explain this fact, even if the H_2 value is obtained through two different analyzers located at two different places in the sampling line.

4.2. Influence of the particle size

Under the explored conditions, the particle diameter is a crucial parameter which significantly affects the results. Fig. 5 shows the temperature evolution of biomass particles of different diameters (0.4 and 1.1 mm, mixture of softwoods) at a nominal reactor temperature of ~1100 K. Small particles quickly reach the gas

Table 2
Comparison between model predictions and experimental yields at the reactor outlet for 0.4 mm particles of softwood and beech.

	Softwoods mixture (0.4 mm)				Beech wood (0.45 mm)			
Temperature	1073 K		1223 K		1073 K		1223 K	
Mass yield (% w)	Exp.	Pred.	Exp.	Pred.	Exp.	Pred.	Exp.	Pred.
H_2	1.2	2.2	1.7	2.2	1.2	2.2	1.9	2.2
CO	43	50	40	47	48	50	49	47
CO_2	7.0	11.4	7.0	10.0	11.3	11.4	10.0	10.0
CH_4	4.4	6.3	4.6	5.1	6.6	6.3	6.6	5.1
C_2H_4	5.0	4.9	3.1	3.0	5.2	4.9	3.0	3.0
C_2H_2	1.1	1.0	2.2	3.4	1.4	1.0	3.3	3.4
C_2H_6	No.mea.	0.5	No.mea.	0	0.8	0.5	0	0
H_2O	11	14	10	12	13	14	12	12

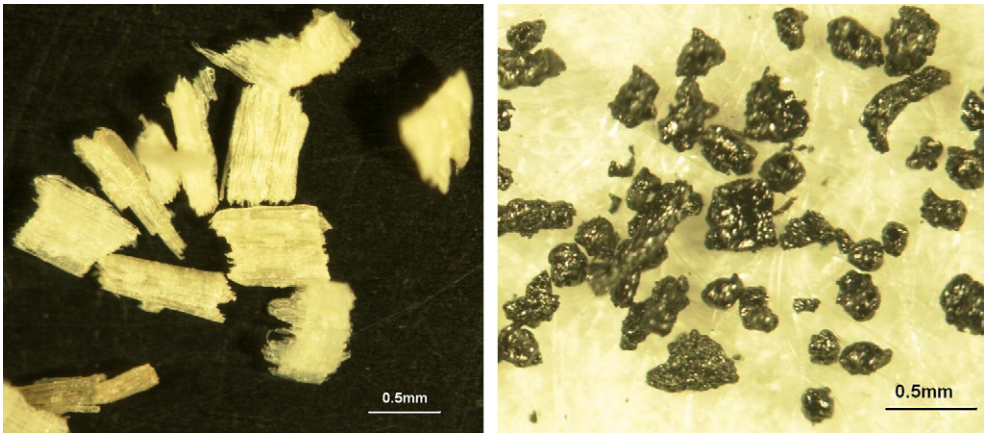

Fig. 6. Particle morphological changes during the pyrolysis in the EFR (softwood particles of 0.4 mm at 1073 K).

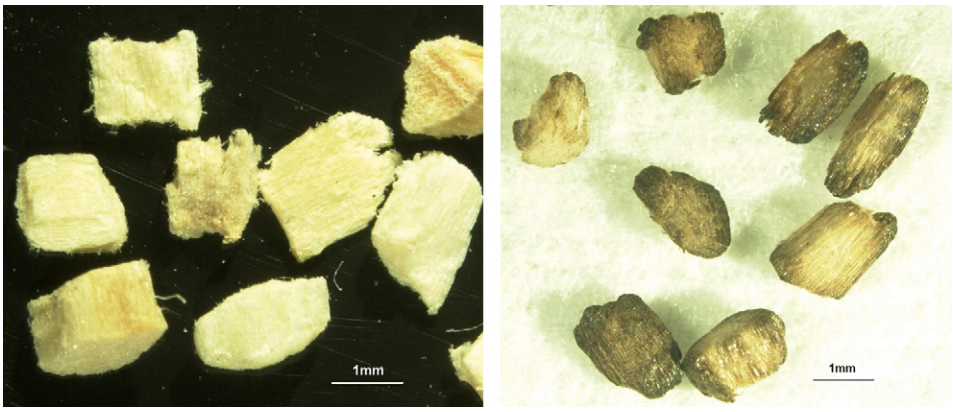

Fig. 7. Particle morphological changes during the pyrolysis in the EFR (softwood particles of 1.1 mm at 1073 K).

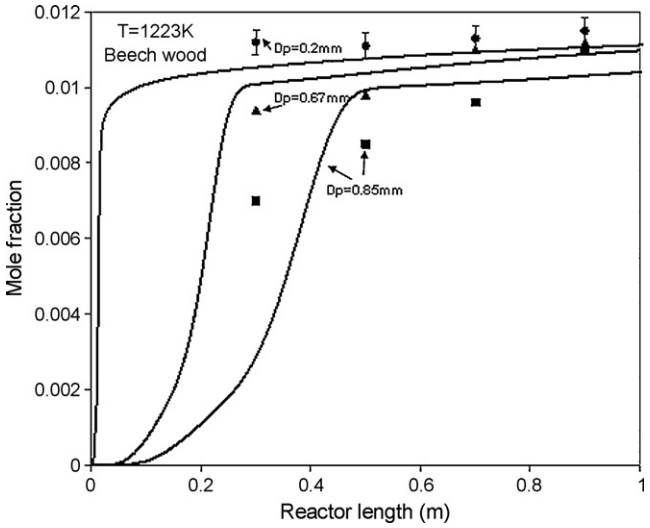

Fig. 8. Comparisons between experimental measurements (points) and model predictions (lines) for CO mole fraction (beech wood particles of 0.20 mm at 1073 K).

temperature, while large particles require a longer residence time. This is mainly due to the higher velocity of the large particles, for which the residence time is too short to reach the gas phase temperature. In particular, the maximal solid residence time for the particles of 0.4 mm is ~2 s while for the particles of 1.1 mm it is ~0.5 s. Moreover, while the temperature of the small particles is practically uniform, significant internal temperature gradients can be seen for the large particles, due to internal thermal resistances.

Although the measurement of temperature profile inside the particle is not available, and possible uncertainties in the determination of heat transfer conditions might partially modify the temperature profiles of Fig. 5, the morphological changes of solid residue from the same biomass of different initial sizes (shown in Figs. 6 and 7) confirm the model calculation. These photos reveal that the large particles (1.1 mm) are only '*toasted*' at moderate temperature at the reactor outlet, while the devolatilization process of the small particles (0.4 mm) is almost completed and *char* formation is quite evident. In fact, the heating of the solid is very fast and the internal transport resistances are negligible for the small particles (up to ~0.4 mm), while it becomes noteworthy for large particles.

Fig. 8 reports the comparisons between experimental measurements and model predictions of the major species CO versus the reactor length, for beech wood particles of different sizes at 1223 K. It can be seen that the CO yield increases when the reactor length is varied from 0.3 to 0.9 m for larger particles, whereas it remains constant for the smallest ones. This confirms that larger particles require longer time for completing the devolatilization process.

4.3. Role of the secondary gas phase reactions

As previously indicated, a detailed reaction scheme has been integrated in the global model to describe the secondary gas phase reactions. The importance of these secondary pyrolysis

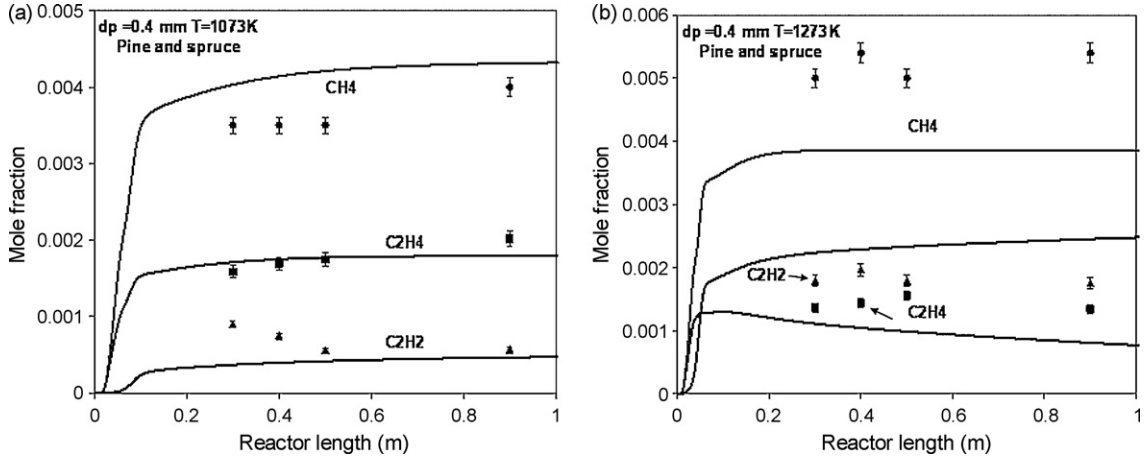

Fig. 9. Comparisons between experimental measurements (points) and model predictions (lines) for softwood particles of 0.40 mm at 1073 K (a) and 1273 K (b).

reactions is confirmed by the experimental observations. For example, C_2H_2 is only the product of the secondary phase dehydrogenation of C_2H_4, and it is favoured by high temperatures [16]. Table 2 and Fig. 9 show that in accordance with the experimental results, model properly predicts this different trend of C_2H_4 and C_2H_2: C_2H_2 is more abundant than C_2H_4 at high temperature, while the reverse behaviour is predicted and experimentally measured at 1073 K.

5. Conclusions

Experiments have been performed at high temperatures (1073–1273 K) and high heating fluxes (10–100 kW m^{-2}) in a lab-scale entrained flow reactor with different wood particles of different sizes. These results have been used to further validate a detailed kinetic model of biomass pyrolysis. The comparisons between experimental results and model prediction show that the main experimental trends are well-reproduced by the model. The crucial influence of the particle size can be seen under the tested operating conditions. For small particles (dp up to 0.4 mm), the decomposition of the biomass components is almost completed after a reactor length of 0.3 m and leads to total gas yields higher than 75 wt% and a char yield of about 10–15 wt% at the reactor outlet. The major gas component is largely CO, followed by H_2. CH_4 and CO_2 are present in smaller amounts. There is a clear effect of temperature on the C_2 species behaviour. For large particles (0.4 mm $<$ dp $<$ 1.1 mm), the decomposition is still under evolution between 0.3 and 0.9 m of reactor length, due to internal heat transfer limitations. These first results and comparisons are encouraging, since the specific fitting for these experiments has been limited. The results prove the real potential of this modelling tool to predict the main product yields and to better understand the complex chemical and physical transformations occurring during biomass pyrolysis inside industrial reactors. For a more complete validation of the model, new experiments are planned in the next future with a more complete product analysis including heavier hydrocarbons, such as benzene.

Acknowledgements

The authors acknowledge the fruitful and continuous discussions with Tiziano Faravelli and Alessio Frassoldati. The authors also acknowledge the useful comments and suggestions of the referees.

References

[1] W. De Jong, G. Di Nola, B.C.H. Venneker, H. Spliethoff, M.A. Wojtowicz, Fuel 86 (2007) 2367–2376.
[2] Y.G. Chen, S. Charpenay, A. Jensen, M.A. Serio, M.A. Wojtowicz, A.C.S. Fuel Chem. Div. Preprints, 1997, 1.
[3] Y.G. Chen, S. Charpenay, A. Jensen, M.A. Wojtowicz, M.A. Serio, Modeling of Biomass Pyrolysis Kinetics, in: Proceedings of the Twenty-Seventh Symposium (International) on Combustion, 1998.
[4] S. Niksa, Predicting the Rapid Devolatilization of Diverse Forms of Biomass with Bio-FLASHCHAIN, in: Proceedings of the Combustion Institute, 2000.
[5] C.D. Sheng, J.L.T. Azevedo, Modeling biomass devolatilization using the chemical percolation devolatilization model for the main components, in: Proceedings of the Combustion Institute, 2002, p. 29.
[6] H.R. Pond, T.H. Fletcher, L.L. Baxter, Prediction of tar and light gas during pyrolysis of black liquor and biomass, in: Proceedings of the Third Annual Joint Meeting of the U.S. Sections of the Combustion Institute, Chicago, 2003.
[7] W.C.R. Chan, M. Kelbon, B.B. Krieger, Fuel 64 (1985) 1505–1513.
[8] M.G. Gronli, A theoretical and experimental study of the thermal degradation of biomass, Faculty of Mechanical Engineering, The Norwegian University of Science and Technology, 1996.
[9] H. Lu, Experimental and Modeling Investigations of Biomass Particle Combustion, Department Chemical Engineering, Brigham Young University, 2006.
[10] M. Bellais, Modelling of the pyrolysis of large wood particles, in: in Department of Chemical Engineering and Technology, Royal Institute of Technology, Stockholm, 2007.
[11] C. Di Blasi, Progress in Energy and Combustion Science 34 (2008) 47–90.
[12] A.M.C. Janse, R.W.J. Werterhout, et al. "Modelling of Flash Pyrolysis of a Single Wood Particle." Chemical Engineering and Processing, 39 (2000) 239–252.
[13] S.R.A. Kersten, et al., Interpretation of biomass gasification by "quasi"-equilibrium models, in: Proceedings of the 12th European Conference on Biomass for Energy, Industry and Climate Protection, Amsterdam, 2002.
[14] X. Wang, S.R.A. Kersten, W. Prins, W.P.M. van Swaaij, Ind. Eng. Chem. Res. 44 (2005) 8786–8795.
[15] E. Ranzi, A. Cuoci, T. Faravelli, A. Frassoldati, G. Migliavacca, S. Pierucci, S. Sommariva, Energy Fuels (2008), doi:10.1021/ef800551t.
[16] J.M. Commandré, P. Gauthier, G. Boissonnet, S. Salvador, D. Schweich, Fuel 87 (2008) 1155–1164.
[17] R. Zanzi, K. Sjostrom, E. Bjornbom, Fuel 75 (1996) 545–550.
[18] S. Li, S. Xu, S. Liu, C. Yang, Q. Lu, Fuel Proc. Technol. 85 (2004) 1201–1211.
[19] C. Dupont, G. Boissonnet, J.-M. Seiler, P. Gauthier, D. Schweich, Fuel 86 (2007) 32–40.
[20] S.R.A. Kersten, et al., Interpretation of biomass by quasi-equilibrium models, in: Proceedings of the Twelfth European Conference on Biomass for Energy, Industry and Climate Protection, Amsterdam, The Netherlands, 2002.
[21] X.T. Li, J.R. Grace, C.J. Lim, A.P. Watkinson, H.P. Chen, J.R. Kim, Biomass Bioenergy 26 (2004) 171–193.
[22] E. Ranzi, M. Dente, A. Goldaniga, G. Bozzano, T. Faravelli, Prog. Energy Combust. Sci. 27 (2001) 99–139.
[23] C. Branca, C. Di Blasi, H. Horacek, Ind. Eng. Chem. Res. 41 (2002) 2107–2114.
[24] G. Buzzi-Ferraris, D. Manca, Comput. Chem. Eng. 22 (1998) 1595–1621.
[25] G. Buzzi-Ferraris, Numerical Libraries in C++. 2007. Available from: http://www.chem.polimi.it/homes/gbuzzi.
[26] S. Pierucci, E. Ranzi, ESCAPE 18 Comput. Aided Process Eng. 25 (2008) 901–906.
[27] C. Dupont, Vapogazéification de la biomasse: contribution à l'étude de la phénoménologie entre 800 et 100ÔC. 2006, Université Claude Bernard, Lyon 1, Lyon.
[28] W.E. Ranz, W.R. Marshall, Chem. Eng. Prog. 48 (1952) 141–146, 173-180.
[29] R.B. Bird, W.E. Stewart, E.N. Lightfoot, Transport Phenomena, 2nd ed., Wiley, New York, 2002.